PHARMACEUTICAL BIOLOGY
2022, VOL. 60, NO. 1, 1264–1277
https://doi.org/10.1080/13880209.2022.2086584

Taylor & Francis
Taylor & Francis Group

RESEARCH ARTICLE

OPEN ACCESS Check for updates

Anti-liver fibrosis effects of the total flavonoids of litchi semen on CCl_4-induced liver fibrosis in rats associated with the upregulation of retinol metabolism

Jiongyi Yan[a,b*], Yinyi Feng[a*‡], Xuewan Fang[a], Xiaojuan Cui[a], Xing Xia[a], Fang Li[a§], Weisheng Luo[a], Jianqin Liang[a§], Jianfang Feng[a§] and Kai Yu[c]

[a]College of Pharmacy, Guangxi University of Chinese Medicine, Nanning, China; [b]School of Health, Wuzhou Vocational College, Wuzhou, China; [c]College of Animal Science and Technology, Guangxi University, Nanning, China

ABSTRACT

Context: The litchi semen are traditional medications for treating liver fibrosis (LF) in China. The mechanism remains unclear.

Objective: This study investigates the anti-liver fibrotic mechanism of the total flavonoids of litchi semen (TFL).

Materials and methods: Sprague-Dawley rats with carbon tetrachloride-induced LF were treated with TFL (50 and 100 mg/kg) for 4 weeks. The anti-liver fibrotic effects of TFL were evaluated and the underlying mechanisms were investigated via histopathological analysis, proteomic analysis and molecular biology technology.

Results: Significant anti-LF effects were observed in the high-TFL-dose group (TFL-H, $p < 0.05$). Five hundred and eighty-five and 95 differentially expressed proteins (DEPs) were identified in the LF rat model (M group) and TFL-H group, respectively. The DEPs were significantly enriched in the retinol metabolism pathway ($p < 0.0001$). The content of 9-*cis*-retinoic acid (0.93 ± 0.13 vs. 0.66 ± 0.10, $p < 0.05$, vs. the M group) increased significantly in the TFL-H group. The upregulation of RXRα (0.50 ± 0.05 vs. 0.27 ± 0.13 protein, $p < 0.05$), ALDH2 (1.24 ± 0.09 vs. 1.04 ± 0.08 protein, $p < 0.05$), MMP3 (0.89 ± 0.02 vs. 0.61 ± 0.12 protein, $p < 0.05$), Aldh1a7 (0.20 ± 0.03 vs. 0.03 ± 0.00 mRNA, $p < 0.05$) and Aox3 (0.72 ± 0.14 vs. 0.05 ± 0.01 mRNA, $p < 0.05$) after TFL treatment was verified.

Conclusions: TFL exhibited good anti-liver fibrotic effects, which may be related to the upregulation of the retinol metabolism pathway. TFL may be promising anti-LF agents with potential clinical application prospects.

ARTICLE HISTORY
Received 23 August 2021
Revised 11 April 2022
Accepted 1 June 2022

KEYWORDS
9-*Cis*-retinoic acid; iTRAQ; liver disease; RXRα; traditional Chinese medicine

Introduction

Liver fibrosis (LF), a wound-healing reaction of the liver to liver injury, is a necessary stage of chronic liver disease leading to cirrhosis, which is associated with excessive extracellular matrix (ECM) deposition (Huang et al. 2017). As a worldwide health problem, LF can develop into cirrhosis, liver cancer and liver failure and is associated with significant morbidity and mortality during liver injury (Zhang et al. 2019). Several studies have shown that LF, and early cirrhosis, can be reversed by prompt initiation of treatment (Sun and Kisseleva 2015; Chen et al. 2018; Du et al. 2019). Therefore, it is particularly important to treat LF before it develops into cirrhosis or liver cancer. At present, the pathogenesis of LF remains unclear. Clinically, there is a lack of specific and effective Western medications to treat LF, and whose side effects are obvious (Shan et al. 2019). Therefore, it is necessary to understand the pathogenesis of LF to identify more effective drugs. Traditional Chinese medications have unique advantages, such as synergistic effects, low toxicity and enhanced safety, and demonstrate great potential for the treatment of LF.

Litchi is the mature fruit of *Litchi chinensis* Sonn. (Sapindaceae), which is widely distributed in Southeast Asia, especially in Southern China (Zhao et al. 2020). The seeds of litchi are used as a traditional Chinese medication. In recent decades, practitioners of traditional Chinese medicine have used the tablet and powder forms of litchi semen to treat LF and cirrhosis. Modern pharmacological studies have demonstrated that litchi semen possess various pharmacological activities, such as liver protection (Dong et al. 2018), antioxidation (Wang et al. 2011), hypoglycaemic (Man et al. 2017; Tang et al. 2018), antitumor and neuralgia-relieving activities (Chung et al. 2017; Guo et al. 2017). Flavonoids are the main active components of litchi semen. In our previous study, we isolated and purified the total flavonoids of litchi semen (TFL) from litchi semen and verified that they exerted good anti-LF effects and improved liver

CONTACT Jianqin Liang 80004622@qq.com; Jianfang Feng fengjianfang@vip.163.com No. 13 Wuhe Road, Qingxiu District, Guangxi University of Chinese Medicine, Nanning 530200, Guangxi, China; Kai Yu yukai@st.gxu.edu.cn No. 100 East Daxue Road, Xixiangtang District, Guangxi University, Nanning 530004, Guangxi, China
*Both authors contributed equally to this work.
‡Sixth Affiliated Hospital of Guangxi Medical University, Yulin, China.
§South China Branch of National Engineering Research Center for Manufacturing Technology of Traditional Chinese Medicine Solid Preparation, Nanning, China.

Supplemental data for this article can be accessed online at https://doi.org/10.1080/13880209.2022.2086584

© 2022 The Author(s). Published by Informa UK Limited, trading as Taylor & Francis Group.
This is an Open Access article distributed under the terms of the Creative Commons Attribution-NonCommercial License (http://creativecommons.org/licenses/by-nc/4.0/), which permits unrestricted non-commercial use, distribution, and reproduction in any medium, provided the original work is properly cited.

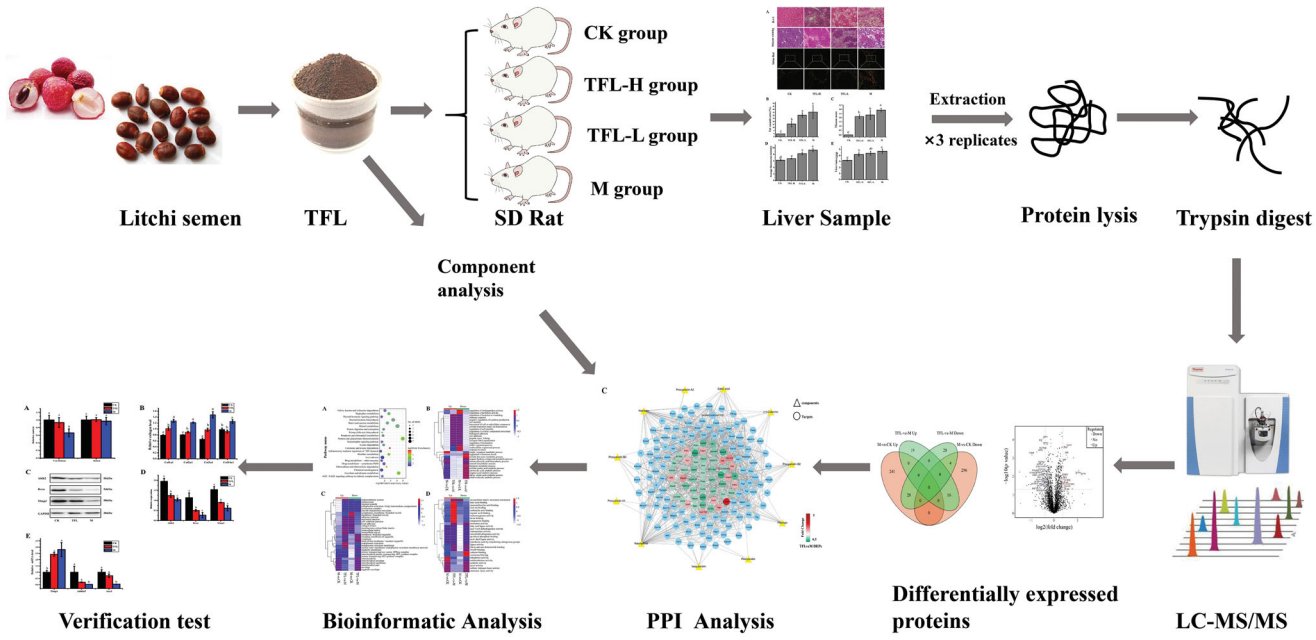

Figure 1. Overall flowchart of the study.

function using animal experiments (Huang et al. 2016). However, the mechanisms underlying the anti-LF effects of TFL remain unclear.

In recent years, proteomic technologies have emerged as powerful tools to detect, analyse and determine changes in the expression of disease-related proteins after drug treatment; therefore, they offer one of the most effective techniques to study the molecular mechanisms of drug action. At present, the isobaric tags for relative and absolute quantification (iTRAQ) technique are used to study many chronic liver diseases, such as LF (Dong et al. 2016), liver cirrhosis (Minghui et al. 2019) and liver cancer (Goh et al. 2011; Buczak et al. 2018).

In this study, a rat model of CCl_4-induced LF was established to reveal the underlying mechanisms of TFL in the treatment of LF at a large-scale protein level. After TFL treatment, iTRAQ was used to detect differentially expressed proteins (DEPs) in rat liver tissues, and the key targets and pathways were examined, thus providing a new perspective on the pathogenesis of LF and the therapeutic mechanism of TFL (Figure 1).

Materials and methods

Extraction, purification and chemoprofile of TFL

Litchi semen were collected from Yulin (Guangxi Autonomous Region, China), in May 2018, and were taxonomically confirmed by Professor Songji Wei of Guangxi University of Chinese Medicine. The voucher specimen (20180510) was maintained in Guangxi University of Chinese Medicine. Litchi semen were crushed and refluxed thrice with an eight-fold volume of 60% ethanol for 30 min. After the ethanol extract was filtered, the filtrates were combined, concentrated and dried, and a reddish-brown crude extract of TFL was obtained. Thereafter, the crude extract was dissolved in 20% ethanol, separated and purified using an AB-8 macroporous resin column to obtain TFL.

The components of TFL were analysed using UPLC-Q-Exactive spectrometry (UPLC, Dionex UltiMate 3000, Dionex, Sunnyvale, CA; MS, Q-Exactive, Thermo Fisher Scientific, Waltham, MA). Chromatographic separation was achieved using a Hypersil GOLD C18 column (2.1 × 50 mm, 1.9 μm; Thermo Fisher Scientific, Waltham, MA, 25002-052130) at 30 °C. The mobile phase consisted of a gradient mixture of methanol and 0.1% formic acid in water. Q-Exactive was operated in the Full MS/dd-MS2 mode with a resolution of 70,000. The standard substances used for qualitative analysis of TFL included procyanidin, procyanidin A1, procyanidin A2, procyanidin B2, procyanidin B3, phlorizin, nobiletin, (+)-catechin, gallic acid, kaempferol and isoquercitrin.

The content of procyanidin A2 in TFL was determined using HPLC (Shimadzu, Kyoto, Japan). Chromatographic separation was achieved using an Ultimate AQ-C18 column (4.6 mm × 250 mm, 5 μm; Welch, Concord, MA, 00207-31043) at 30 °C. The mobile phase consisted of methanol and 0.1% phosphoric acid (20:80, v/v), and a flow rate of 1.0 mL/min was used. The sample injection volume was 10 μL.

The purity of TFL was determined using a UV–Vis spectrophotometer (Shimadzu UV-2600, Kyoto, Japan). The purified extract solution was sequentially reacted with 5% (w/v) vanillin and concentrated hydrochloric acid (Taniguchi et al. 2007). The optical density was measured at 510 nm on a UV–Vis spectrophotometer, and procyanidin A2 was used as the reference standard for the external standard calibration.

Establishment of a rat model of LF and treatment

Male Sprague-Dawley (SD) rats, weighing 220–230 g, were provided by the Hunan SJA Laboratory Animal Co., Ltd. (licence no. SCXK [Xiang] 2016-0002). The rats were housed under controlled conditions (25 ± 2 °C, 75 ± 5% humidity, on a 12-h light/dark cycle) and had free access to rodent chow and water. All experimental procedures and protocols used in this study were approved by the Institutional Review Board of Guangxi University of Chinese Medicine. All experimental animals were raised in the Animal Experimental Centre of Guangxi University of Chinese Medicine.

After acclimatization for three days, the rats were randomly divided into the control (CK, $n = 10$) and model (M, $n = 48$) groups. Rats in the M group were injected with 3 mL/kg CCl_4

(2:3, mixed with soybean oil) twice a week, and those in the CK group were injected with 3 mL/kg soybean oil. From the sixth week of modelling, six rats from the M group were sacrificed every week. Masson's staining was used to detect collagenous fibres in liver tissues to ensure successful establishment of the LF model. If the average LF score was >2.5, LF was considered to be successfully induced. Thereafter, rats with LF were randomly divided into the M, high-TFL-dose (TFL-H) and low-TFL-dose (TFL-L) groups, with 10 rats in each group. All rats in the M and TFL group were injected with CCl_4 at a maintenance dose of 3 mL/kg once a week, whereas those in the CK group were injected with 3-mL/kg soybean oil once a week. In addition, rats in the M and CK groups were intragastrically administered 5-mL/kg normal saline, and those in the TFL-L and TFL-H groups were administered 50 and 100 mg/kg TFL. All rats were treated for 4 weeks.

Calculation of the liver index

Liver samples were rinsed with NS, wiped with filter paper and weighed. The liver index was calculated using the following formula:

$$\text{Liver index} = [\text{liver weight (g)}/\text{body weight (g)}] \times 100\%$$

Examination of pathological changes in liver samples

Liver tissues were fixed in the same position using 4% paraformaldehyde, processed using standard histological procedures, embedded in paraffin blocks and cut into 4-μm-thick sections. Some slices were stained with haematoxylin and eosin (H&E) to observe pathological injuries, whereas other slices were stained with Masson and Sirius red to observe the abundance of collagen and its different types. Pathological changes in the liver samples were observed using a microscopic camera. The scoring criteria used for calculating the LF degree are shown in Table 1 (Wang et al. 2015).

Protein preparation, iTRAQ labelling and LC–MS/MS analysis

As the pharmacological effects of the TFL-H group were better than those of the TFL-L group, the TFL-H group was selected for proteomic analysis. Nine liver tissues from the CK, TFL-H and M groups were randomly divided into three replicates. First, the liver tissues were ground to powder in liquid nitrogen, dissolved in a lysis buffer [8-M urea (Vetec, Rio de Janeiro, Brazil, V900119], 2-mM ethylenedinitrilotetraacetic acid (Vetec, Rio de Janeiro, Brazil, V900106) and 10-mM DL-dithiothreitol [Vetec, Rio de Janeiro, Brazil, V900830)] and 1% protease inhibitor cocktail (Amresco, Solon, OH, M222) for protein extraction and centrifuged after ultrasonication to obtain the supernatant. Thereafter, acetone (Sangon, A6854, Shanghai, China) at a volume three-times that of the supernatant was added to the supernatant to precipitate the protein. After centrifugation and removal of the supernatant, the protein precipitate was redissolved in urea buffer [8-M urea and 100-mM triethylammonium bicarbonate (Thermo Fisher Scientific, Waltham, MA)], and protein concentration was determined using a Bradford Protein Assay Kit (Beyotime, P0006, Shanghai, China).

For peptide isotope labelling, 100 μg of protein was reduced and alkylated. Thereafter, sequencing-grade trypsin (Pierce, San Jose, CA, 90057) was added at a protein:trypsin mass ratio of 50:1 and incubated at 37 °C overnight for protein digestion and subsequently at a ratio of 100:1 for 4 h for depth digestion. After enzymolysis, the peptides were desalted using a Strata X SPE column (Phenomenex, Torrance, CA, 8B-S100-AAK) and dried under vacuum. Eventually, the peptides were labelled with iTRAQ Reagent-8Plex (Applied Biosystems Sciex, Framingham, MA, 4381663) according to the manufacturer's protocol. The CK, M and TFL groups were labelled with reagents 113, 114 and 121, respectively. The peptide mixture was incubated at room temperature for 2 h, collected in a tube and dried using vacuum centrifugation.

The iTRAQ-labelled peptide mixtures were redissolved in solvent A (2% ACN, pH 10) of HPLC and directly loaded onto a high-pH reverse-phase column (130 Å, 3.5 μm, 4.6 × 250 mm) (Waters, Milford, MA, Bridge Peptide BEH C18). A total of 18 fractions were collected and desalted using Ziptip C18 (Millipore, Burlington, MA, ZTC18S096) according to the manufacturer's instructions, dried under vacuum and analysed qualitatively and quantitatively using LC–MS/MS. First, the peptides were separated on an EASY-nLC 1000 ultra-performance liquid-phase system and analysed on a Thermo Q-Exactive mass spectrometer. High-resolution Orbitrap was used to detect and analyse the parent ion and secondary fractions. Data were acquired using a data-dependent scanning (DDA) program.

The resulting MS/MS spectra were searched against the UniProt proteome database of *Rattus norvegicus* (UP000002494, downloaded on 15 December 2017, including 29,795 sequences) by integrating SEQUEST data in the Proteome Discoverer software (version 1.3, Thermo Fisher Scientific, Waltham, MA). The database parameters were set as follows: the enzyme was set as trypsin/P, and two missed cleavages were allowed. Carbamidomethyl (C) was selected as a fixed modification, and iTRAQ 8plex (N-term), iTRAQ 8plex (K, Y) and oxidation were selected as variable modifications. For protein identification and quantification, a peptide segment mass tolerance of 10 ppm and a fragment ion tolerance of 0.05 Da were permitted, and the false discovery rate of peptide filtration was set to 0.05.

Annotation and functional classification

The target sites were identified using the SwissTargetPrediction (http://www.swisstargetprediction.ch/) database. For bioinformatic analyses of differential proteins and targets in the TFL group, Gene Ontology (GO) analysis was performed using Database for Annotation, Visualization and Integrated Discovery (DAVID, v6.8) (http://david.abcc.ncifcrf.gov/), Kyoto Encyclopedia of Genes and Genomes (KEGG) pathway annotation was performed using KAAS (https://www.genome.jp/tools/kaas/) and the KEGG Mapper tool was used for visualization. A protein–protein interaction (PPI) network was constructed using the STRING database and visualized using the Cytoscape software (version 3.7.1).

Table 1. Scoring criteria used for Masson's staining of the liver tissues of rats with LF.

Scoring criteria	Score
Normal	0
Fibrosis present (collagen fibres present that extend from the portal triad or central vein to the peripheral region)	1
Mild fibrosis (mild collagen fibres present with extension but without compartment formation)	2
Moderate fibrosis (moderate collagen fibres present with some pseudo lobe formation)	3
Severe fibrosis (many collagen fibres present with thickening of the partial compartments and frequent pseudo lobe formation)	4

Western blot

Total protein was isolated from liver tissues using a tissue protein extraction kit (Solarbio, Beijing, China, BC3711) and centrifuged at 15,000×*g* for 30 min at 4 °C. Protein concentration was measured using a BCA Protein Assay Kit (Beyotime, P0010S, Shanghai, China). Furthermore, proteins (30 μg) were separated using sodium dodecyl sulphate-polyacrylamide gel electrophoresis (SDS-PAGE), with a 10% gel, and subsequently transferred onto a polyvinylidene fluoride (PVDF) membrane. Thereafter, the membrane was blocked with 5% dried skim milk for 2 h at 4 °C. The blot was washed with TBST and incubated overnight at 4 °C with the polyclonal primary antibodies MMP3 (1:20,000; Abcam, Cambridge, UK), Aldh2 (1:10,000; Abcam, Cambridge, UK), GAPDH (1:10,000; Thermo Fisher Scientific, Waltham, MA) and Rxrα (1:10,000; Abcam, Cambridge, UK) diluted in TBST, followed by incubation with the horseradish peroxidase-conjugated secondary antibody goat anti-rabbit IgG (1:5000) at 4 °C for 2 h. Protein expression was detected using an ultra-sensitive ECL chemiluminescence kit, and images were captured using a gel imaging system (Bio-Rad, Hercules, CA). Band intensity was analysed using the ImageJ software (Bethesda, MD), and the results were normalized to those of GAPDH, which was used as the internal control.

qRT-PCR

Total RNA was extracted from liver tissues using an RNAprep Pure Tissue kit (Tiangen, Beijing, China, DP431) and reverse transcribed to cDNA using a qRT-PCR kit (Vazyme, Nanjing, China, R223-01). The relative mRNA levels were determined using quantitative PCR. The PCR parameters were as follows: 95 °C for 3 min, followed by 45 denaturation cycles at 95 °C for 10 s, annealing at 57 °C for 10 s (GAPDH, 55 °C) and extension at 72 °C for 20 s. The target mRNA levels were adjusted to those of GAPDH, which was used as the endogenous control. The fold change values relative to the control values were obtained and used to represent the changes in gene expression. The PCR primers designed using Primer 5.0 are shown in Table 2.

Determination of the content of retinol and 9-cis-retinoic acid in liver samples

Retinol (2 mg) and 9-*cis*-retinoic acid (2 mg) were respectively dissolved in 2 mL methanol to prepare reference solution. Liver tissue (0.1 g) was collected, added to an appropriate amount of methanol and homogenized. The homogenate was ultrasonicated for 20 min and centrifuged at 13,000×*g* for 10 min at 4 °C. The supernatant was filtered using a 0.22-μm microporous membrane, and relative quantitative analysis was performed using HPLC–MS/MS. Chromatographic separation was achieved using a Hypersil GOLD C18 column (2.1 × 50 mm, 1.9 μm; Thermo Fisher Scientific, Waltham, MA, 25002-052130) at 30 °C. The mobile phase consisted of a gradient mixture of methanol and 0.1% formic acid in water. The Q-Exactive spectrometer was operated in the Full MS/dd-MS2 mode with a resolution of 70,000.

Table 2. Primer sequences used for gene expression.

Target gene	Primer sequence
GAPDH	(F) GACATGCCGCCTGGAGAAAC
	(R) AGCCCAGGATGCCCTTTAGT
Timp1	(F) TGGCATCCTCTTGTTGCTATCA
	(R) AACGCTGGTATAAGGTGGTCTC
Aldh1a7	(F) GGCAGCCATCTCTTCTCACAT
	(R) ACAGCACTATCCAAGTCAGCAT
Aox3	(F) TAACCAGCAGCAAGCCACAT
	(R) GCGAGCATACGAGTCAGCA

Statistical analyses

Data were expressed as mean ± standard deviation of the mean. Statistical analyses were performed using the Statistical Package for the Social Sciences software (SPSS, Chicago, IL), version 13.0. Statistical analysis of the histological scores was performed using Student's *t*-test. A p value <0.05 was considered statistically significant, and proteins with a threshold of >1.3-fold or $<1/1.3$-fold and a p value <0.05 were classified as DEPs.

Results

Chemoprofile of TFL

A total of 11 components of TFL were identified via UPLC (as shown in Table S1). Most components belonged to the proanthocyanidin class of flavonoids, such as procyanidin A1, A2, B2 and B3. The content and purity of procyanidin A2 (determined using procyanidin A2 equivalents) in TFL were 0.923 mg/g and 65%, respectively.

Histopathological changes in liver tissues

The liver index is usually used to indicate the extent of liver damage. The liver index of the M group was significantly higher than that of the CK group ($p < 0.01$); however, after TFL treatment, the liver index of the TFL-H group was remarkably lower than that of the M group ($p < 0.01$). The results revealed that TFL alleviated CCl_4-induced hepatic intumescence in rats (Figure 2(E)).

Furthermore, to investigate the protective effects of TFL against LF, histological changes in the liver tissues of rats were detected using H&E and Masson's staining. The results obtained using H&E staining in the CK group showed a normal hepatic lobular architecture and no inflammatory cells. In addition, inflammatory cell infiltration and the number of fat vacuoles around hepatocytes were significantly increased in the M group after 12 weeks of CCl_4 stimulation. After TFL treatment, pathological changes in liver tissues, especially the number of fat vacuoles, were significantly reduced in the TFL-H group but not in the TFL-L group ($p < 0.05$) (Figure 2(A,B)). Based on the results of Masson's staining, there was no fibrosis in the liver tissues of the CK group; however, the structure of the hepatic lobule was destroyed in liver tissues of the M group, accompanied by proliferative fibrous tissue, a large fibrous septum and a pseudolobule. However, in the TFL-H and TFL-L groups, fewer fibrous septa were observed in the liver tissues, and the degree of LF was decreased ($p < 0.05$) (Figure 2(A,C)).

During the development of LF, the composition of the liver ECM changes from type IV collagen to type I and III collagen (Chen et al. 2019). Therefore, to distinguish between the microscopic types of collagens, Sirius red staining was performed. The results of Sirius red staining were similar to those of Masson's staining (Figure 2(A,D)). Under a polarized light microscope, type I collagen showed strong birefringence and yellow or red fibres, whereas type III collagen showed weak birefringence and green fibres. The expression of collagen in the M group was significantly higher than that in the CK group ($p < 0.0001$); however, it was significantly reduced after TFL treatment ($p < 0.01$).

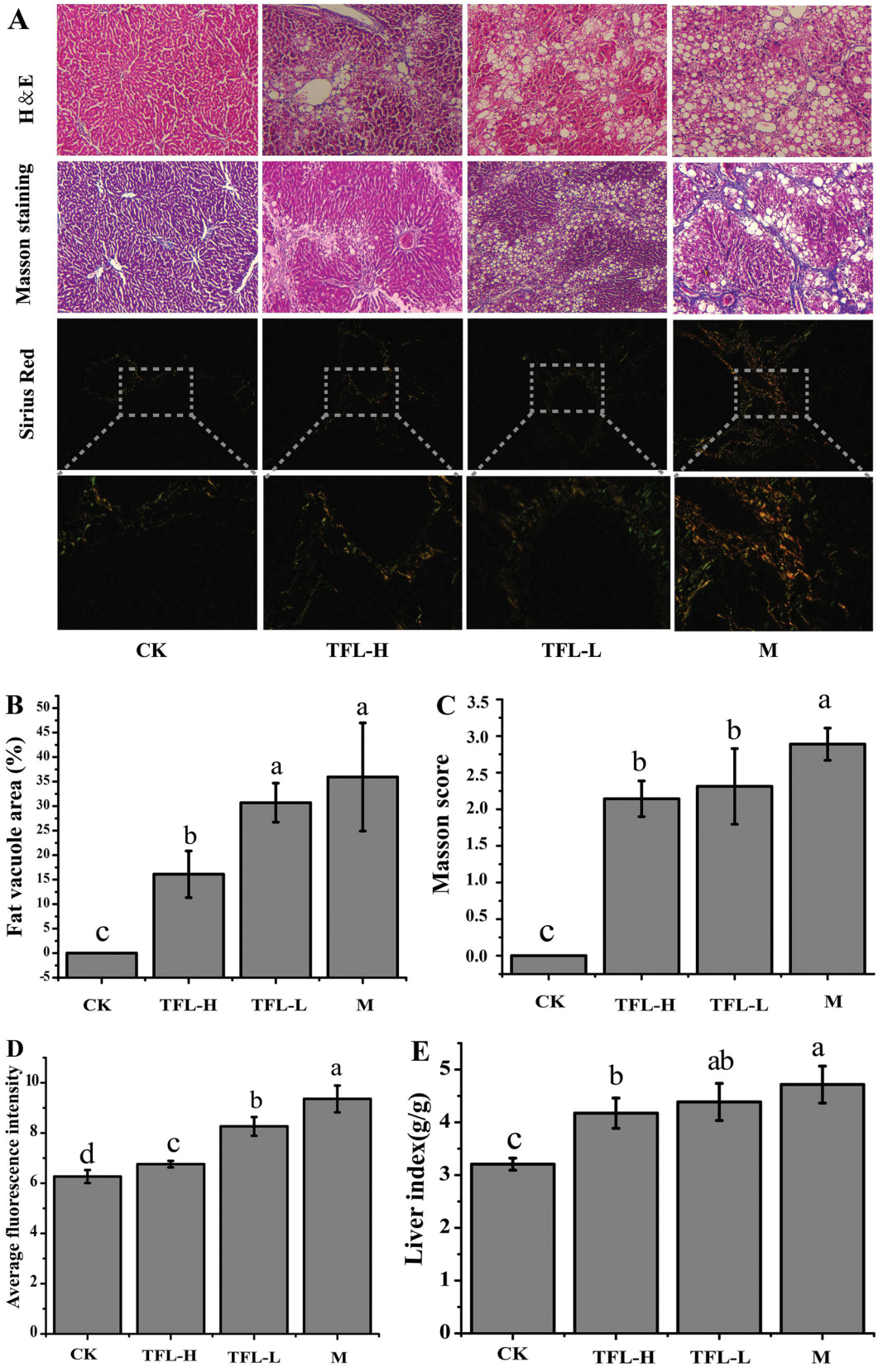

Figure 2. Effects of TFL on the histological changes of liver tissues in rats with CCl_4-induced LF. (A) H&E staining (×100), Masson's staining (×100), and Sirius red staining (×200) of the rat liver tissues (type I collagen is represented in yellow or red, and type III collagen is represented in green). (B) Fat vacuole area analysis using H&E staining. (C) Masson's staining score. (D) Average Sirius red staining intensity. (E) Liver index of different groups.

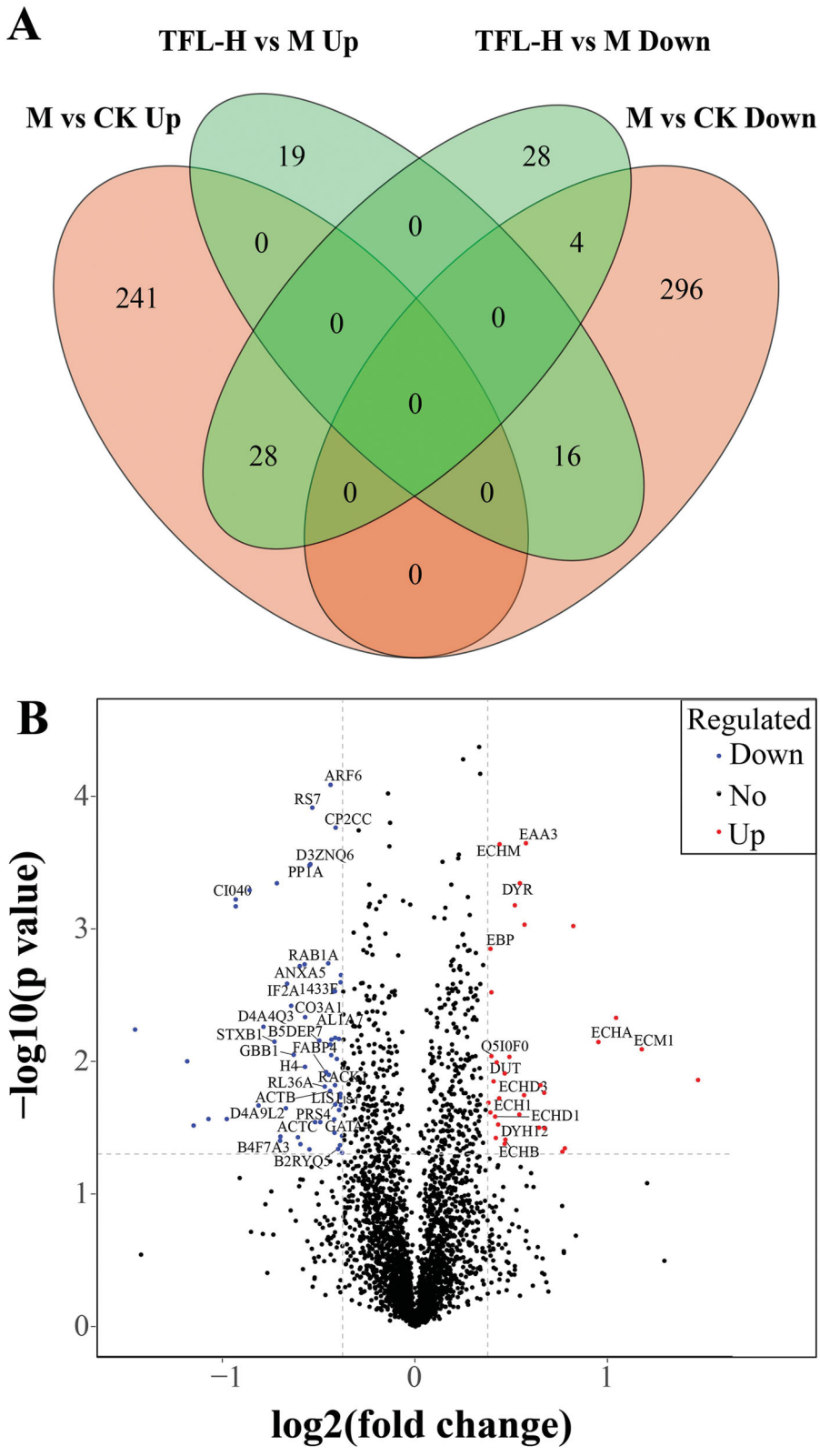

Figure 3. Overview of the DEPs identified using iTRAQ and PPI network analysis. (A) Venn diagram of overlapping regulatory proteins in the TFL-H versus M groups and the M versus CK groups. (B) Volcano map of DEPs in the TFL-H versus M groups. The names of proteins with a threshold of >2-fold or <0.5-fold are shown. (C) The component–target network.

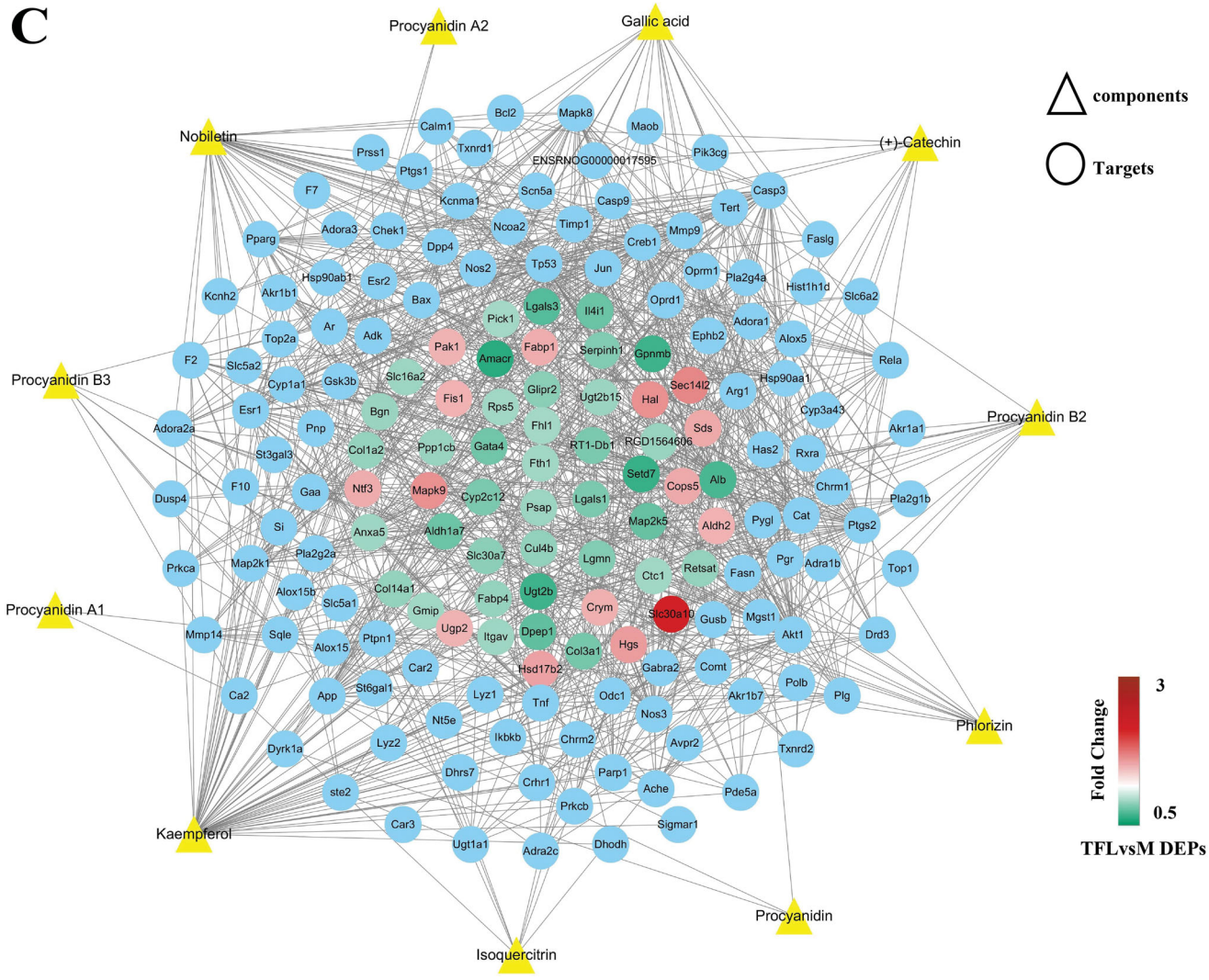

Figure 3. Continued.

Identification of DEPs and PPI network analysis

To identify DEPs and the targets of TFL in LF rat models, proteins extracted from the rat liver samples were assessed using LC–MS/MS, followed by isotope labelling using iTRAQ. A total of 6004 proteins were identified, and DEPs were designated at a threshold of >1.3-fold (upregulated) or <1/1.3-fold (downregulated) with a p value <0.05. Based on these cut-off values, we found that the expression of 585 and 95 proteins was significantly different in the CK and TFL-H groups, respectively, when compared with the M group. The Venn diagram demonstrated that 316 proteins were downregulated in the M group compared with the CK group; of which, 16 were upregulated after TFL treatment (Figure 3(A)), whereas 269 proteins were upregulated in the M group compared with the CK group; of which, 28 were downregulated after TFL treatment. The names of proteins with a threshold of >2-fold or <0.5-fold and a p value <0.05 are shown in the volcano map demonstrating DEPs in the TFL-H and M groups (Figure 3(B)).

To analyse the possible multi-component and multi-target mechanisms of TFL in the treatment of LF, the TCMSP and SwissTargetPrediction databases were used to screen for the targets of the above-mentioned 11 TFL components, and the possible interactions between the components and targets were analysed and visualized using Cytoscape (version 3.7.1) (Shannon et al. 2003). A total of 109 potential targets of TFL components (blue) were screened and analysed based on the DEPs of the TFL-H and M (red and green) groups to establish a component–target interaction network (Figure 3(C)). Different components of the network interacted with the same or different targets. Kaempferol and nobiletin interacted with the largest number of targets.

Clustering and functional analysis of DEPs

The KEGG pathway analysis was performed to assess the involvement of DEPs in metabolic or signalling pathways. The DEPs of the TFL-H and M groups were mainly enriched in retinol metabolism, pentose and glucuronate interconversion, drug metabolism (cytochrome P450), steroid hormone biosynthesis and other pathways (Figure 4(A)). Among these pathways, retinol metabolism was the most enriched pathway. Therefore, we speculated that the anti-fibrotic effects of TFL were closely related to retinol metabolism.

Furthermore, GO functional annotations of the DEPs were classified as biological processes, cellular components and molecular functions. GO enrichment analysis showed that TFL

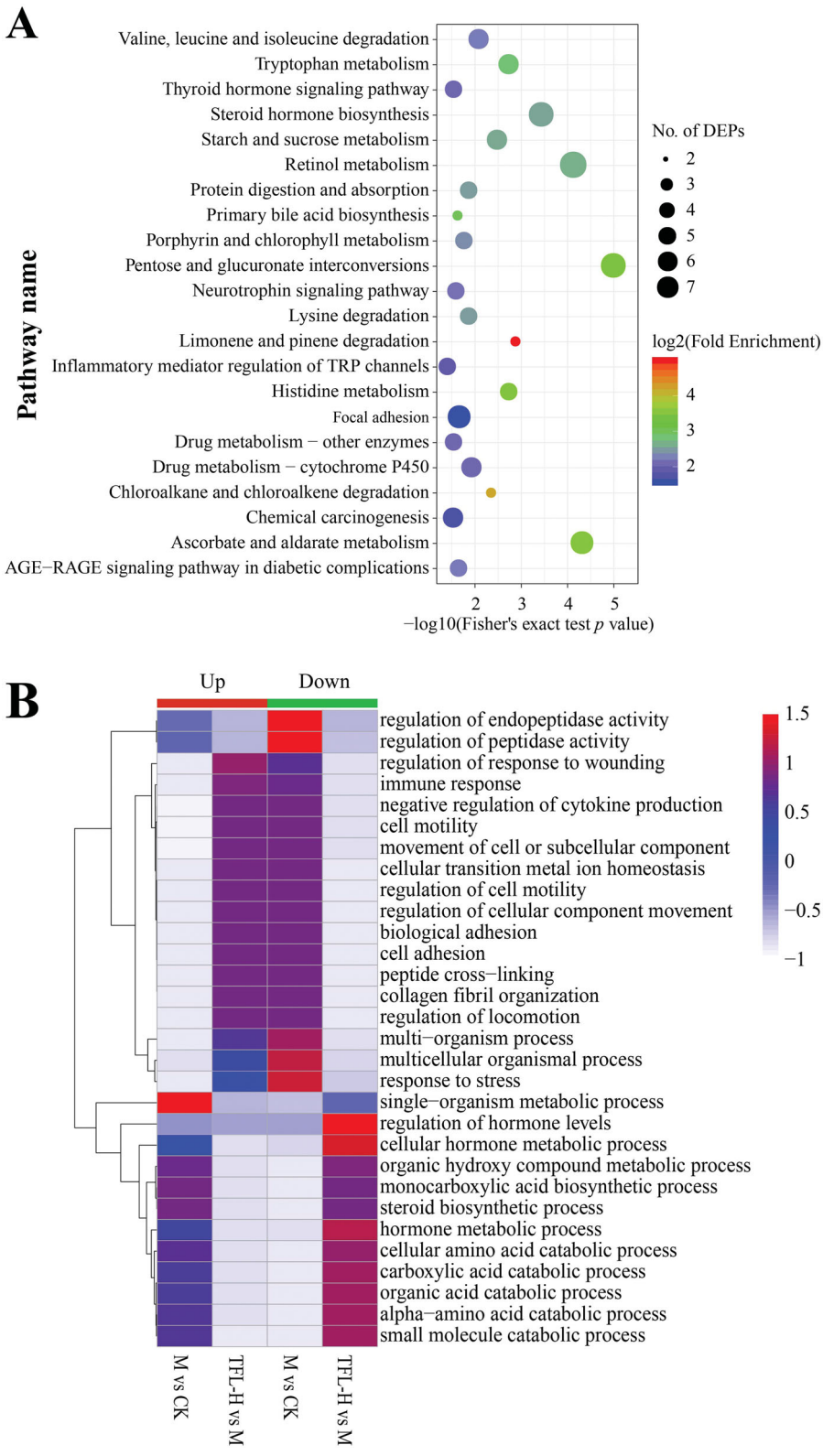

Figure 4. Clustering and functional analysis of DEPs. (A) KEGG analysis of DEPs in the TFL-H versus M groups. (B) GO biological process analysis of DEPs in the TFL-H versus M groups. (C) GO cellular component analysis of DEPs in the TFL-H versus M groups. (D) GO molecular function analysis of DEPs in the TFL-H versus M groups.

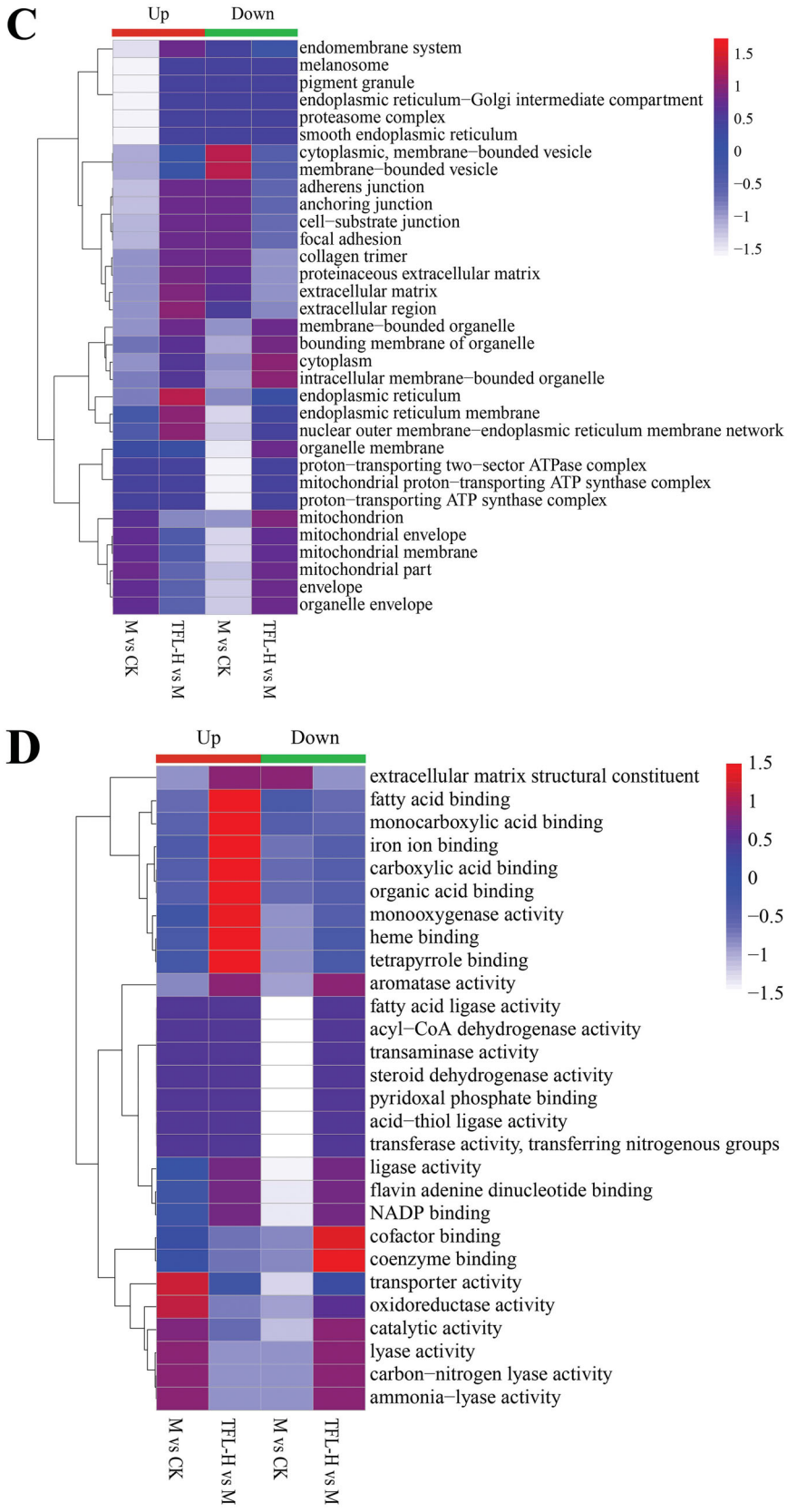

Figure 4. Continued.

treatment mainly affected the immune response, negative regulation of cytokine production and α-amino acid catabolism (Figure 4(B)). In addition, significant changes were observed in the expression of ECM proteins, extracellular domain and organelle binding membrane (Figure 4(C)). Moreover, molecular functions, such as fatty acid-binding, coenzyme-binding and oxidoreductase activities, changed significantly (Figure 4(D)). These results indicated that the anti-fibrotic effects of TFL might be related to

ECM deposition and lipid metabolism, which are regulated by the retinol metabolism pathway.

Validation of proteins, genes and metabolites related to the retinol metabolism pathway

Retinol metabolism refers to the oxidative metabolism of retinol in the body to produce retinoids, such as retinol, retinoic acid and other analogues, and is closely related to physiological functions of the liver. It not only controls the storage and metabolism of retinol but is also an important target of many retinoids (Shao et al. 2005). In addition, retinol and its metabolites retinaldehyde and retinoic acid are closely related to the occurrence and development of liver diseases. In this study, the content of retinol was lower in the M group than in the CK group; however, the difference was not significant, whereas the content of 9-*cis*-retinoic acid was significantly lower in the M group than in the CK group. After TFL treatment, the content of retinol was slightly increased, whereas that of 9-*cis*-retinoic acid was significantly increased and was equivalent to that in the CK group (Figure 5(A)).

Alterations in retinoic acid metabolism in the liver and abnormalities in the retinoic acid signalling pathway are closely related to liver diseases (Shirakami et al. 2012). A proteomic study found that retinol metabolism-related proteins and various types of collagens were abnormally expressed in rats with LF (Figure 5(B)). In this study, Western blot and qRT-PCR were used to validate the expression of proteins or their corresponding genes screened via proteomic analysis. The expression of Aldh2 protein, Aldh1a7 mRNA and Aox3 mRNA related to retinol metabolism was significantly increased after TFL treatment ($p < 0.05$) (Figure 5(C–E)). Aldh2, Aldh1a7 and Aox3 are the enzymes involved in the conversion of 9-*cis*-retinal to 9-*cis*-retinoic acid, and their increased expression can promote the synthesis of retinoic acid. These results suggested that an increase in the content of 9-*cis*-retinoic acid after TFL treatment was positively correlated with the expression of these enzymes.

In addition, 9-*cis*-retinoic acid interacts with retinoid X receptors (RXRs), such as retinoid X receptor alpha (Rxrα), to regulate the expression of many genes involved in liver metabolism. In this study, the expression of Rxrα increased significantly after TFL treatment, which was consistent with the increased content of 9-*cis*-retinoic acid.

Furthermore, collagen is one of the main constituents of ECM, which is deposited on the liver during LF. Abnormal activity of liver matrix metalloproteinases (Mmps) or tissue inhibitors of Mmps (Timps) leads to an imbalance in ECM degradation (Duarte et al. 2015; Lachowski et al. 2019). In this study, the Mmp3 protein was significantly downregulated, the Timp1 protein was significantly upregulated and the Mmp3/Timp1 ratio was significantly decreased in the M group compared with the CK group. After TFL treatment, although the expression of Timp1 was not significantly decreased, the expression of Mmp3 and the Mmp3/Timp1 ratio were significantly increased (Figure 5(D,E)). In addition, based on the results of Masson's staining, ECM deposition was significantly reduced (Figure 2(A)).

Discussion

Although LF is considered a reversible pathological process, effective drugs are still lacking. Therefore, it is of great significance to understand the pathogenesis of LF for developing more effective drugs for its prevention and treatment. Previous studies have shown that flavonoids are one of the main active components of litchi semen, which have anti-inflammatory, antioxidant and anti-LF effects; however, their specific mechanism and targets of action remain unknown (Cheng et al. 2020). In this study, we investigated the mechanism of action of TFL in CCl_4-induced LF using proteomic techniques. As shown in Figure 2(A,C,E), the pathological analysis verified that TFL effectively reduced CCl_4-induced liver injury, inflammation, fat accumulation and fibrosis. Subsequently, the iTRAQ technique was used to analyse and identify DEPs in rat liver tissue. A total of 585 DEPs were identified in the M and CK groups, which were mainly enriched in metabolic pathways, including valine, leucine and isoleucine degradation and retinol metabolism. Retinol metabolism refers to the oxidative metabolism of vitamin A (i.e., retinol) in the body to produce retinoids, such as retinal, retinoic acid and other analogues. It has been demonstrated that abnormalities in retinol metabolism can lead to non-alcoholic fatty liver disease (NAFLD), non-alcoholic steatohepatitis (NASH) and advanced liver disease (Blaner 2019). In this study, after TFL treatment, the retinol metabolism pathway changed significantly, which was the most enriched pathway of DEPs. These results suggest that retinol metabolism is involved in the occurrence and progression of LF, and the therapeutic effects of TFL on LF in rats may be related to the regulation of retinol metabolism.

Furthermore, we detected the content of retinol and its metabolite, 9-*cis*-retinoic acid. The results revealed no significant differences in the content of retinol in rat liver tissue between the M and CK groups; however, the content of 9-*cis* retinoic acid was significantly lower in the M group (Figure 5(A)). Retinol and its metabolites participate in the development of vision (Belyaeva et al. 2018); the differentiation, proliferation and apoptosis of cells *in vivo* (Doldo et al. 2015; Zhou et al. 2016; Khalil et al. 2017) and the regulation of the immune system (Bono et al. 2016). On the one hand, retinol and its metabolites play an anti-steatotic role by increasing the oxidation of fatty acids and inhibiting the synthesis of fatty acids in the liver. On the other hand, retinoic acid is a key regulator of glucose and lipid metabolism in the liver and adipose tissue (Saeed et al. 2017), which can inhibit the expression of type I collagen in HSCs. Some regulatory factors of retinol metabolism and storage overlap with those of lipid metabolism (related to cholesterol and triglyceride metabolism). When these factors are imbalanced, they lead to disease progression (Blaner 2019). For example, the content of retinol is low in patients with liver cirrhosis (Ukleja et al. 2002) and those with morbid obesity with NAFLD (Botella-Carretero et al. 2010). Moderate administration of vitamin A, synthetic retinoic acid or retinoic acid RARβ2 receptor agonists are beneficial in the treatment of liver diseases (Wang et al. 2007; Trasino et al. 2016; Yeh et al. 2018; Blaner 2019). Therefore, maintaining high levels of retinol and retinoic acid is one of the available methods to prevent and treat liver diseases, including LF. However, it is noteworthy that a diet with an excess of vitamin A or excessive vitamin A doses and alcohol consumption can accelerate the formation of liver normalized (Okuno et al. 2002). In this study, the content of retinoic acid in the rat liver tissue was significantly increased after TFL treatment, which suggested that the therapeutic effects of TFL on LF were related to an increase in the retinoic acid level, which was consistent with the analysis results of the above scholars.

In the retinol metabolism pathway, retinol is converted to retinaldehyde by alcohol dehydrogenase (ADH) in cells, and retinaldehyde is subsequently converted to retinoic acid by

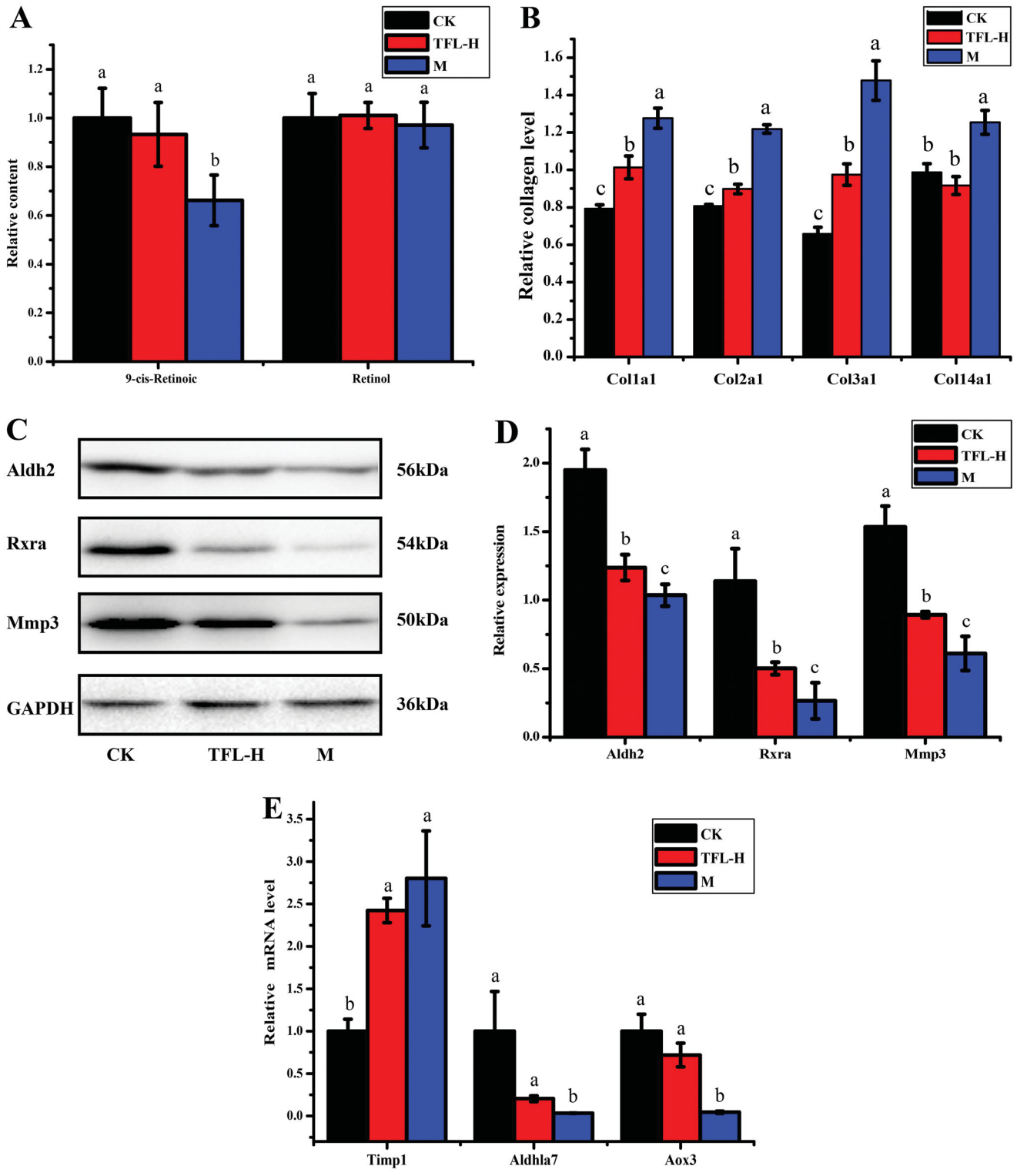

Figure 5. Validation of proteins, genes, and metabolites related to retinol metabolism. (A) The relative content of retinol and 9-*cis* retinoic acid in liver samples. (B) The relative content of Col1a1, Col1a2, Col3a1, and Col14a1 proteins detected via proteomic analysis. (C) Semi-quantitative analysis based on the relative density of the validated proteins. Data were normalized to the results of GADPH, which was used as the internal reference. (D) The expression of Aldh2, Rxrα, and Mmp3 proteins. (E) Relative mRNA expression of Timp1, Aldh1a7, and Aox3.

acetaldehyde dehydrogenase (ALDH) and Aox3 (Zakhari 2006; Kawai et al. 2016). As shown in Figure 4(C–E), TFL group compared with the M group, the expression levels of Aldh2, Aldh1a7 and Aox3 in rat liver tissue were significantly increased after TFL treatment. Therefore, the significant increase in the content of retinol and retinoic acid in rat liver tissue after TFL treatment was associated with the increased expression of Aldh2, Aldh1a7 and Aox3, which promote retinol metabolism.

Moreover, abnormal retinol metabolism is related to abnormal lipid metabolism in LF. Retinoic acids activate the transcriptional networks controlled by retinoic acid receptors (RARs) and RXRs (Huang et al. 2014; Saeed et al. 2017). Animal studies have

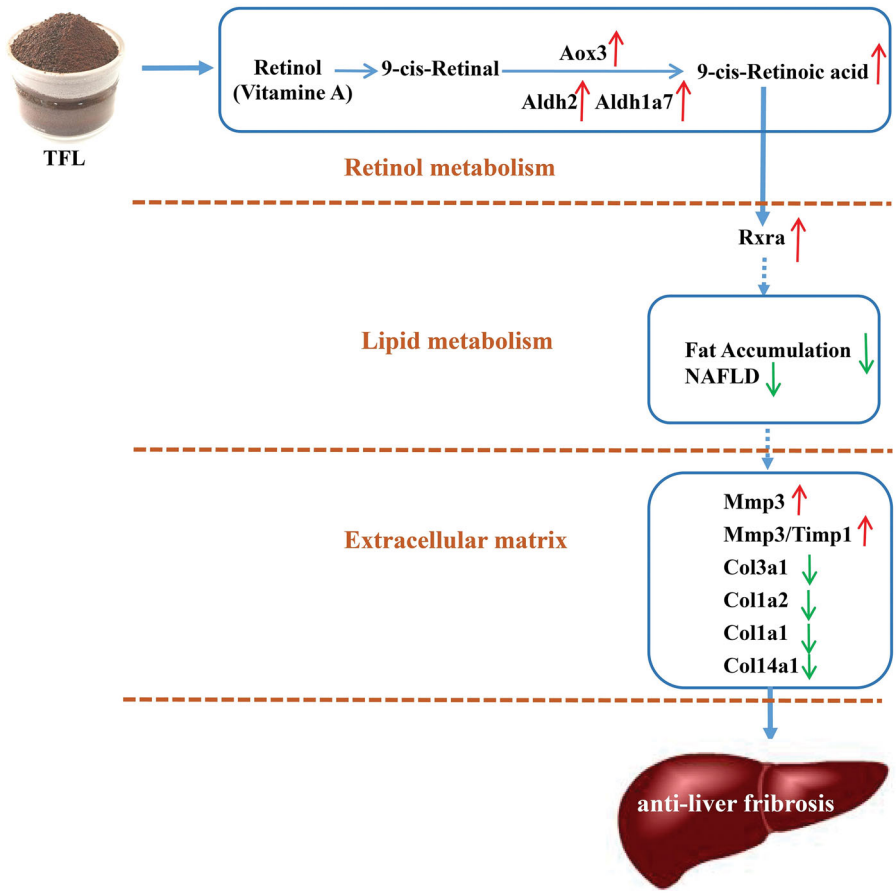

Figure 6. Potential therapeutic mechanisms of TFL in rats with LF.

shown an association between transcription factors (Ppar-α, Rxr-α, Ucp-2 and Srebp-1c) and enzymes involved in lipid metabolism (liver CPT-1 and fatty acid synthase) after retinoid treatment (Pettinelli et al. 2018). Rxrα, the receptor of 9-*cis* retinoic acid downstream of the retinol metabolism pathway, is one of the members of the LXR/RXR signalling cascade, which controls the cholesterol levels in tissues. The LXR/RXR signalling axis influences lipid homeostasis by regulating the expression of related genes (Chi et al. 2019). *In vitro* experiments have revealed that the mRNA levels of Rxrα are significantly decreased during HSC activation (Mezaki et al. 2009). In this study, we observed that the expression of Rxrα was downregulated, fat accumulation was increased in the liver tissue and the fatty liver condition was very serious. After TFL treatment, the expression of Rxrα was upregulated, and the number of fat vacuoles was significantly reduced. These results suggest that the mechanism of action of TFL in the treatment of LF is related to the Rxrα-mediated lipid metabolism pathway, which regulated steatosis and deposition. However, the effects of TFL on lipid metabolism require further investigation.

Benign steatosis can easily develop into hepatic inflammation, which further leads to chronic liver injury, such as NAFLD. Under long-term inflammatory stimulation, such as fatty acid oxidation in the adipose tissue, immune responses and healing continuously occur in hepatocytes, leading to an imbalance between Mmps and Timps, which affects ECM degradation and leads to the development of fibrosis (Saeed et al. 2017). Furthermore, during LF development, the mediators released by damaged liver cells promote the activation of HSCs and their differentiation into myofibroblasts and further produce large amounts of ECM proteins. Collagen I and III, which are the main components of ECM, are synthesized by fibroblasts, and their excessive secretion and accumulation are pathological features of LF (Mahmoud et al. 2019). As shown in Figures 5(B) and 2(A), after TFL treatment, the expression of Col1a1, Col1a2, Col3a1 and Col14a1 proteins and the total expression of collagen I and collagen III were significantly reduced ($p < 0.01$). As shown in Figure 5(D,E), after TFL treatment, although the expression of Timp1 was not significantly decreased, the expression of Mmp3 and the Mmp3/Timps ratio was significantly increased. These results suggested that TFL inhibited the proliferation of fibroblasts as well as the production and deposition of ECM proteins, which further inhibits LF progression. The potential therapeutic mechanisms of TFL in rats with LF are shown in Figure 6.

This study helps to further elucidate the underlying mechanisms of TFL in ameliorating changes in overall protein levels in rat models of LF. Furthermore, identification of various DEPs is beneficial for the discovery and selection of novel drug targets for LF. However, owing to limited time and financial support, multiple targets and pathways of TFL against LF could not be experimentally validated.

Conclusions

TFL effectively alleviated CCl_4-induced LF in rats. The mechanism of action is related to the upregulation of retinol metabolism, which consequently affects lipid metabolism and ECM degradation. These results suggest that TFL is a promising anti-LF agent with potential clinical applications.

Acknowledgements

The authors would like to thank all colleagues who contributed to this study.

Author contributions

Jianfang Feng, Jianqin Liang and Kai Yu designed the study. Jiongyi Yan and Yinyi Feng performed experiments and wrote the main manuscript. Xuewan Fang, Xiaojuan Cui, and Fang Li performed animal experiments. Xing Xia, and Weisheng Luo analysed the data.

Disclosure statement

The authors declare no conflict of interest.

Funding

This study was supported by the National Natural Science Foundation of China under Grant Number [81960872]; Innovation-Driven Development Project of Guangxi under Grant number [GUIKE AA17202035]; Graduate Education Innovation Program of Guangxi University of Chinese Medicine under Grant number [YCXJ2021012]; Young and Middle Teachers' Basic Ability Improvement Project of Guangxi under Grant number [2022KY1500]; and Guangxi Science and Technology Base and Talent Project under Grant number [GUIKE AD20238058].

ORCID

Jiongyi Yan http://orcid.org/0000-0001-8170-9182
Jianqin Liang http://orcid.org/0000-0003-2755-8680
Kai Yu http://orcid.org/0000-0001-5338-3437

Data availability statement

The data used to support the findings of this study are available from the corresponding author upon request.

References

Belyaeva OV, Wu L, Shmarakov I, Nelson PS, Kedishvili NY. 2018. Retinol dehydrogenase 11 is essential for the maintenance of retinol homeostasis in liver and testis in mice. J Biol Chem. 293(18):6996–7007.

Blaner WS. 2019. Vitamin A signaling and homeostasis in obesity, diabetes, and metabolic disorders. Pharmacol Ther. 197:153–178.

Bono MR, Tejon G, Flores-Santibañez F, Fernandez D, Rosemblatt M, Sauma D. 2016. Retinoic acid as a modulator of T cell immunity. Nutrients. 8(6): 349–364.

Botella-Carretero JI, Balsa JA, Vázquez C, Peromingo R, Díaz-Enriquez M, Escobar-Morreale HF. 2010. Retinol and alpha-tocopherol in morbid obesity and nonalcoholic fatty liver disease. Obes Surg. 20(1):69–76.

Buczak K, Ori A, Kirkpatrick JM, Holzer K, Dauch D, Roessler S, Endris V, Lasitschka F, Parca L, Schmidt A, et al. 2018. Spatial tissue proteomics quantifies inter- and intratumor heterogeneity in hepatocellular carcinoma (HCC). Mol Cell Proteomics. 17(4):810–825.

Chen X, Li WX, Chen Y, Li XF, Li HD, Huang HM, Bu FT, Pan XY, Yang Y, Huang C, et al. 2018. Suppression of SUN2 by DNA methylation is associated with HSCs activation and hepatic fibrosis. Cell Death Dis. 9(10):1021–1031.

Chen Z, Jain A, Liu H, Zhao Z, Cheng K. 2019. Targeted drug delivery to hepatic stellate cells for the treatment of liver fibrosis. J Pharmacol Exp Ther. 370(3):695–702.

Cheng QC, Qin W, Zhuo L, Zhao YZ, Fan LW, Lin WS, Liu RB. 2020. Comparison of total flavone of *Litchi chinensis* Sonn in two kinds of hepatic fibrosis model of rats. Her Med. 39:1179–1184.

Chi L, Lai Y, Tu P, Liu CW, Xue J, Ru H, Lu K. 2019. Lipid and cholesterol homeostasis after arsenic exposure and antibiotic treatment in mice: potential role of the microbiota. Environ Health Perspect. 127(9):97002.

Chung YC, Chen CH, Tsai YT, Lin CC, Chou JC, Kao Y, Huang CC, Cheng CH, Hsu CP. 2017. Litchi seed extract inhibits epidermal growth factor receptor signaling and growth of two non-small cell lung carcinoma cells. BMC Complement Altern Med. 17(1):16–24.

Doldo E, Costanza G, Agostinelli S, Tarquini C, Ferlosio A, Arcuri G, Passeri D, Scioli MG, Orlandi A. 2015. Vitamin A, cancer treatment and prevention: the new role of cellular retinol binding proteins. Biomed Res Int. 2015:624627.

Dong S, Chen QL, Song Y, Sun Y, Wei B, Li XY, Hu YY, Liu P, Su SB. 2016. Mechanisms of CCl_4-induced liver fibrosis with combined transcriptomic and proteomic analysis. J Toxicol Sci. 41(4):561–572.

Dong XZ, Wang YH, He XJ. 2018. Antioxidant chemical constituents from lychee seed (*Litchi chinensis* Sonn.). J Complement Altern Med Res. 5(3): 1–10.

Du X-S, Li H-D, Yang X-J, Li J-J, Xu J-J, Chen Y, Xu Q-Q, Yang L, He C-S, Huang C, et al. 2019. Wogonin attenuates liver fibrosis via regulating hepatic stellate cell activation and apoptosis. Int Immunopharmacol. 75: 105671.

Duarte S, Baber J, Fujii T, Coito AJ. 2015. Matrix metalloproteinases in liver injury, repair and fibrosis. Matrix Biol. 44–46:147–156.

Goh WW, Lee YH, Zubaidah RM, Jin J, Dong D, Lin Q, Chung MCM, Wong L. 2011. Network-based pipeline for analyzing MS data: an application toward liver cancer. J Proteome Res. 10(5):2261–2272.

Guo H, Luo H, Yuan H, Xia Y, Shu P, Huang X, Lu Y, Liu X, Keller E, Sun D, et al. 2017. Litchi seed extracts diminish prostate cancer progression via induction of apoptosis and attenuation of EMT through Akt/GSK-3β signaling. Sci Rep. 7:41656.

Huang H, Kang Y, Huang XP, Wang CX, Luo WS. 2016. Effect of total flavone from *Litchi chinensis* Sonn on Smad3, Smad4 and TIMP-1 expression in a rat model of liver fibrosis. World Chin J Dig. 2:176–186.

Huang P, Chandra V, Rastinejad F. 2014. Retinoic acid actions through mammalian nuclear receptors. Chem Rev. 114(1):233–254.

Huang Y, Deng X, Liang J. 2017. Modulation of hepatic stellate cells and reversibility of hepatic fibrosis. Exp Cell Res. 352(2):420–426.

Kawai T, Yanaka N, Richards JS, Shimada M. 2016. *De novo*-synthesized retinoic acid in ovarian antral follicles enhances FSH-mediated ovarian follicular cell differentiation and female fertility. Endocrinology. 157(5): 2160–2172.

Khalil S, Bardawil T, Stephan C, Darwiche N, Abbas O, Kibbi AG, Nemer G, Kurban M. 2017. Retinoids: a journey from the molecular structures and mechanisms of action to clinical uses in dermatology and adverse effects. J Dermatolog Treat. 28(8):684–696.

Lachowski D, Cortes E, Rice A, Pinato D, Rombouts K, del Rio Hernandez A. 2019. Matrix stiffness modulates the activity of MMP-9 and TIMP-1 in hepatic stellate cells to perpetuate fibrosis. Sci Rep. 9(1):9.

Mahmoud AM, Hozayen WG, Hasan IH, Shaban E, Bin-Jumah M. 2019. Umbelliferone ameliorates CCl_4-induced liver fibrosis in rats by upregulating PPARγ and attenuating oxidative stress, inflammation, and TGF-β1/Smad3 signaling. Inflammation. 42(3):1103–1116.

Man S, Ma J, Yao J, Cui J, Wang C, Li Y, Ma L, Lu F. 2017. Systemic perturbations of key metabolites in type 2 diabetic rats treated by polyphenol extracts from *Litchi chinensis* seeds. J Agric Food Chem. 65(35): 7698–7704.

Mezaki Y, Yamaguchi N, Yoshikawa K, Miura M, Imai K, Itoh H, Senoo H. 2009. Insoluble, speckled cytosolic distribution of retinoic acid receptor alpha protein as a marker of hepatic stellate cell activation *in vitro*. J Histochem Cytochem. 57(7):687–699.

Minghui Z, Kunhua H, Yunwen B, Hongmei L, Jing L, Shaowen W, Longqiaozi S, Chaohui D. 2019. Analysis of differentially expressed proteins involved in autoimmune cirrhosis and normal serum by iTRAQ proteomics. Prot Clin Appl. 13(3):1700153.

Okuno M, Kojima S, Akita K, Matsushima-Nishiwaki R, Adachi S, Sano T, Takano Y, Takai K, Obora A, Yasuda I. 2002. Retinoids in liver fibrosis and cancer. Front Biosci. 7(1–3):d204–d218.

Pettinelli P, Arendt BM, Teterina A, McGilvray I, Comelli EM, Fung SK, Fischer SE, Allard JP. 2018. Altered hepatic genes related to retinol metabolism and plasma retinol in patients with non-alcoholic fatty liver disease. PLOS One. 13(10):e0205747.

Saeed A, Dullaart RPF, Schreuder T, Blokzijl H, Faber KN. 2017. Disturbed vitamin A metabolism in non-alcoholic fatty liver disease (NAFLD). Nutrients. 10(1):29–53.

Shan L, Liu Z, Ci L, Shuai C, Lv X, Li J. 2019. Research progress on the anti-hepatic fibrosis action and mechanism of natural products. Int Immunopharmacol. 75:105765.

Shannon P, Markiel A, Ozier O, Baliga NS, Wang JT, Ramage D, Amin N, Schwikowski B, Ideker T. 2003. Cytoscape: a software environment for integrated models of biomolecular interaction networks. Genome Res. 13(11):2498–2504.

Shao RX, Otsuka M, Kato N, Taniguchi H, Hoshida Y, Moriyama M, Kawabe T, Omata M. 2005. Acyclic retinoid inhibits human hepatoma cell growth by suppressing fibroblast growth factor-mediated signaling pathways. Gastroenterology. 128(1):86–95.

Shirakami Y, Lee SA, Clugston RD, Blaner WS. 2012. Hepatic metabolism of retinoids and disease associations. Biochim Biophys Acta. 1821(1): 124–136.

Sun M, Kisseleva T. 2015. Reversibility of liver fibrosis. Clin Res Hepatol Gastroenterol. 39:60–63.

Tang Y, Yu C, Wu J, Chen H, Zeng Y, Wang X, Yang L, Mei Q, Cao S, Qin D. 2018. Lychee seed extract protects against neuronal injury and improves cognitive function in rats with type II diabetes mellitus with cognitive impairment. Int J Mol Med. 41:251–263.

Taniguchi S, Kuroda K, Doi K-i, Inada K, Yoshikado N, Yoneda Y, Tanabe M, Shibata T, Yoshida T, Hatano T. 2007. Evaluation of gambir quality based on quantitative analysis of polyphenolic constituents. Yakugaku Zasshi. 127(8):1291–1300.

Trasino SE, Tang XH, Jessurun J, Gudas LJ. 2016. Retinoic acid receptor β2 agonists restore glycaemic control in diabetes and reduce steatosis. Diabetes Obes Metab. 18(2):142–151.

Ukleja A, Scolapio JS, McConnell JP, Spivey JR, Dickson RC, Nguyen JH, O'Brien PC. 2002. Nutritional assessment of serum and hepatic vitamin A levels in patients with cirrhosis. JPEN J Parenter Enteral Nutr. 26(3): 184–188.

Wang L, Lou G, Ma Z, Liu X. 2011. Chemical constituents with antioxidant activities from litchi (*Litchi chinensis* Sonn.) seeds. Food Chem. 126(3): 1081–1087.

Wang L, Potter JJ, Rennie-Tankersley L, Novitskiy G, Sipes J, Mezey E. 2007. Effects of retinoic acid on the development of liver fibrosis produced by carbon tetrachloride in mice. Biochim Biophys Acta. 1772(1):66–71.

Wang Y, Wang R, Wang Y, Peng R, Wu Y, Yuan Y. 2015. Ginkgo biloba extract mitigates liver fibrosis and apoptosis by regulating p38 MAPK, NF-κB/IκBα, and Bcl-2/Bax signaling. Drug Des Devel Ther. 9:6303–6317.

Yeh YT, Lin NC, Yeh YC, Tsai HL, Chen CY, Liu CP, Liu C. 2018. Vitamin A can ameliorate fibrosis of liver in an established rat model of biliary atresia and Kasai portoenterostomy. J Pediatr Surg. 53(12):2416–2422.

Zakhari S. 2006. Overview: how is alcohol metabolized by the body? Alcohol Res Health. 29:245–254.

Zhang H, Chen Q, Dahan A, Xue J, Wei L, Tan W, Zhang G. 2019. Transcriptomic analyses reveal the molecular mechanisms of schisandrin B alleviates CCl_4-induced liver fibrosis in rats by RNA-sequencing. Chem Biol Interact. 309:108675.

Zhao L, Wang K, Wang K, Zhu J, Hu ZY. 2020. Nutrient components, health benefits, and safety of litchi (*Litchi chinensis* Sonn.): a review. Compr Rev Food Sci Food Saf. 19(4):2139–2163.

Zhou N, Yao Y, Ye H, Zhu W, Chen L, Mao Y. 2016. Abscisic-acid-induced cellular apoptosis and differentiation in glioma via the retinoid acid signaling pathway. Int J Cancer. 138(8):1947–1958.